Perturbation-controlled numerical simulations of the convection onset in a supercritical fluid layer

G. Accary[1,2,*] and H. Meyer[3]

[1]*MSNM-GP, UMR 6181 CNRS, IMT - La Jetée - Technopôle de Château-Gombert, 38 rue Frédéric Joliot Curie, 13451 Marseille, France*

[2]*Faculté des Sciences et de Génie Informatique, Université Saint-Esprit de Kaslik, B.P. 446 Jounieh, Lebanon*

[3]*Department of Physics, Duke University, Durham, North Carolina 27708-0305, USA*

(Received 1 April 2006; published 26 October 2006)

This paper reports 2D and 3D direct numerical simulations of the Rayleigh-Bénard convection in a fluid layer, ^{3}He, close to its gas-liquid critical point. The main quantity of interest is the time when the convective motion becomes appreciable after the heat current has been started. A space periodic, time-independent temperature perturbation is applied to the top plate aiming to represent the various sources of noise in the experiments. A single amplitude of this additional perturbation reproduces the noise level of the experiments for all the used combinations of the critical point proximity and of the heating power. Over four decades of the Rayleigh number, this simple operation removes the systematic discrepancy reported in an earlier paper and brings the simulations into good agreement with the measurements. Scaling of the exponential convection growth rate is presented and discussed.

DOI: 10.1103/PhysRevE.74.046308 PACS number(s): 44.25.+f, 47.27.te, 64.70.Fx

I. INTRODUCTION

In the past five years, many two-dimensional (2D) numerical studies [1–3] were devoted to the convection onset in a Rayleigh-Bénard (RB) cell filled with ^{3}He close to its gas-liquid critical point and heated from below with a current q. Initially, the fluid is on its critical isochore, at a constant temperature T_i slightly above the critical temperature T_c =3.318 K, such that $T_i=(1+\varepsilon)T_c$, where $\varepsilon>0$ defines the dimensionless proximity to the critical point. These simulations correspond to the experiments [4,5] carried out in a flat cylindrical cell of height $H=1.06$ mm and having an aspect ratio (diameter/height) of 54. In the experiment, the fluid layer lies between two horizontal plates made of ultrapure OFHC (oxygen-free high conductivity) copper; these plates are about $10H$ thick ($\sim$1 cm). Given the very large thermal diffusivity of OFHC copper at 3 K ($\sim$3500 cm^2/s), the two plates have a very small thermal inertia in comparison with that of the fluid, with a thermal equilibration time of the order of 0.3 ms. Consequently, only the fluid domain is considered in these simulations. Once the current q is turned on, the temperature difference ΔT between the bottom plate and the top one increases with time, an evolution accelerated by thermoacoustic effects, the so-called "piston effect" [6]. Assuming that the heating is intense enough to induce the hydrodynamic instability of the fluid layer, convective plumes are generated and $\Delta T(t)$ reaches a maximum at $t=t_p$ when these plumes reach the top plate. This instant is followed by damped oscillations of $\Delta T(t)$, specific to a very compressible fluid [2], toward a steady-state heat transfer described by a Rayleigh number defined by

$$\mathrm{Ra}^{\mathrm{corr}} = \frac{g\rho_c^2\beta_P C_P H^4}{\lambda\mu}\left(\frac{\Delta T}{H} - \frac{\Delta T_{\mathrm{ad}}}{H}\right), \tag{1}$$

where $\Delta T=\Delta T_{\mathrm{ss}}$ (steady state), g is the gravity acceleration, ρ_c=41.4 Kg/m^3 is the critical density, λ is the thermal conductivity, β_P is the thermal expansion coefficient, μ is the dynamic viscosity, and C_P is the heat capacity at constant pressure. $\Delta T_{\mathrm{ad}}/H=gT_i\beta_P/C_P$ is the adiabatic temperature gradient [7], which corrects the classical expression of the Rayleigh number by accounting for the diverging compressibility of the fluid as the critical point is approached. Good agreement was obtained between the simulations and the experiments for the period of oscillations of $\Delta T(t)$ and for ΔT_{ss}; however, systematic discrepancies were obtained for the time t_p when the convective regime starts [8].A recent 2D numerical study [3] showed how a temperature perturbation on the top plate accelerates the convection onset, bringing the simulation into a better agreement with the simulation for ε =0.2 and q=0.216 μW/cm^2. And very recently, a semianalytical study [9] established a scaled relation $t_p/\tau_D \sim F(\mathrm{Ra}^{\mathrm{corr}}-\mathrm{Ra}_c)$ for the beginning of the convective regime, where Ra_c=1708 [10] is the critical Rayleigh number and τ_D is the thermal diffusion relaxation time (see Table I in Ref. [8]). For a weakly compressible fluid ($\varepsilon>1$), $\tau_D=H^2/D_T$ (D_T being the thermal diffusivity), but the ratio $\tau_D/(H^2/4D_T)$ decreases with ε from 4 to 1 as $\varepsilon\to 0$.

Besides presenting the first 3D simulations of the problem, this work aims to generalize the idea of the additional perturbation for many values of ε and q, reproducing in the simulations the noise level of the experiments. We consider a space-periodic, time-independent temperature perturbation on the top plate that, according to [3], is effective in speeding up the development of convection. Hence in the 2D approximation, the temperature of the top plate, initially maintained at T_i [1,2], is now assigned $T_{\mathrm{top}}=T_i+B\cos(2\pi y/\alpha H)$, where B is the amplitude of the perturbation of wavelength α (de-

*Corresponding author: gilbertaccary@usek.edu.lb

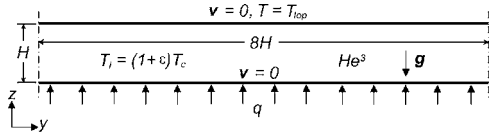

FIG. 1. Supercritical He^3 layer heated from below.

fined below) and y is the horizontal coordinate. The adopted strategy consists in finding the amplitude B that, for the case considered in [3] ($\varepsilon=0.2$ and $q=0.216\ \mu W/cm^2$), yields the best agreement for t_p with the experiment. This amplitude, noted B_{best}, is then used in the modified simulations for various combinations of ε and q.

II. MODELING

The mathematical model is based on the classical Navier-Stokes and energy equations written in the low Mach number approximation. The thermodynamic equilibrium of the fluid is described by a linearized equation of state, and its properties are a function of ε. The model is solved using a finite volume method, accurate to second order in space and to third order in time [11]. A Cartesian computational domain of height $H=1.06$ mm is used together with an aspect ratio of 8, as in [3], with lateral periodic conditions and no-slip vertical boundaries (Fig. 1). As the Rayleigh number at the steady-state increased, the mesh was refined from (120×46) points (in the 2D approximation) up to (240×90) and the time-step was reduced from $0.125s$ to $0.01s$. For example, for $\varepsilon=0.2$ and $q=0.216\mu W/cm^2$, a grid of (160×50) points (uniform in the horizontal direction and refined at the walls) and a time-step of $0.125s$ were sufficient to obtain a mesh and time-step independent solution. While maintaining the top plate at its initial temperature (T_{top}), the simulation is started without heating ($q=0$) and is carried out as the temperature equilibration takes place diffusively throughout the fluid layer in the presence (or absence) of the temperature perturbation on the top plate. After reaching a steady state, the simulation is continued with a constant current q applied on the bottom plate; this instant when the heating starts is chosen to be $t=0$.

As mentioned in the Introduction, the bottom plate has a very high thermal diffusivity that maintains its temperature homogeneous. This property was reproduced numerically by considering along the bottom plate a very thin sublayer, of thickness $h\sim H/1000$, in which the numerical diffusion fluxes in the horizontal directions are artificially increased: the value of the thermal diffusivity D_T^H used to compute these fluxes is gradually increased from D_T (at $z=h$) up to AD_T (with $A\gg1$) at the bottom plate (at $z=0$), as shown in Fig. 2. However, for $h/H\leq10^{-3}$ and $A\geq10^6$, the solution was shown to become independent of these two parameters.

III. RESULTS AND DISCUSSION FOR $\varepsilon=0.2$ AND $q=0.216\ \mu W/cm^2$

A. Temperature fields and time evolution of ΔT

For $\varepsilon=0.2$ and $q=0.216\ \mu W/cm^2$, Fig. 3 shows the evolution of $\Delta T(t)$ with or without additional perturbation on the

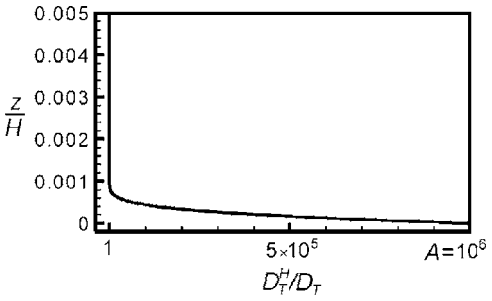

FIG. 2. Distribution of D_T^H in the vicinity of the bottom plate (for $h/H=10^{-3}$ and $A=10^6$) making its temperature homogeneous.

top plate. The unperturbed 2D and 3D solutions were obtained with the same numerical conditions. The perturbed 2D solution was obtained for $\alpha=2$, which corresponds to the wavelength of the temperature field of the unperturbed solution (see Fig. 4, $t=250$ s). Figure 4 shows that the solution is 3D at the convection onset and 2D in the steady state. With $\Delta T_{ss}=87.8\ \mu K$ one obtains $Ra^{corr}=2145$, but as the Rayleigh number increases (for example, for $\varepsilon=0.05$ and $q=45.8\ nW/cm^2$, $Ra^{corr}=4580$), the solution remains 3D in the steady state (see Fig. 5). For still higher Rayleigh numbers, the solution continues evolving with time, hence it remains unsteady. However, a statistically steady state of heat transfer is always reached with a quasiconstant value $\Delta T=\Delta T_{ss}$. For the $\Delta T(t)$ plot, the difference between the 2D approximation and the 3D solution is very small as far as t_p is concerned, and the value of ΔT_{ss} remains the same (it is 6% lower than the experimental value). The small amplitude B of the perturbation ($B\ll\Delta T_{ss}$) does not alter the value of ΔT_{ss}, and consequently that of Ra^{corr} in the steady state, but it leads to a considerable decrease in t_p.

B. Results analysis

In order to better understand the time evolution of ΔT, the enstrophy field [12] was computed. It reflects the intensity of the convective activity, and is defined by

$$\text{Ens}=\sum_{i,j=1}^{3}\frac{1}{2}(\nu_{i,j}-\nu_{j,i})^2, \tag{2}$$

where $\nu_{i,j}$ represents the derivative of the velocity component ν_i in the direction j. Figure 6 shows the time evolutions

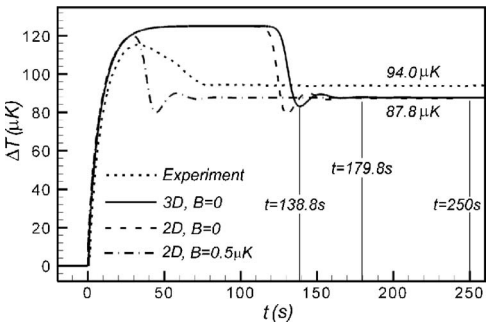

FIG. 3. Time evolution of the temperature difference $\Delta T(t)$ across the fluid layer for $\varepsilon=0.2$ and $q=0.216\ \mu W/cm^2$, with ($B\neq0$) and without ($B=0$) perturbation of the temperature of the top plate. The heating starts at $t=0$. The temperature fields for the indicated instants are shown in Fig. 4.

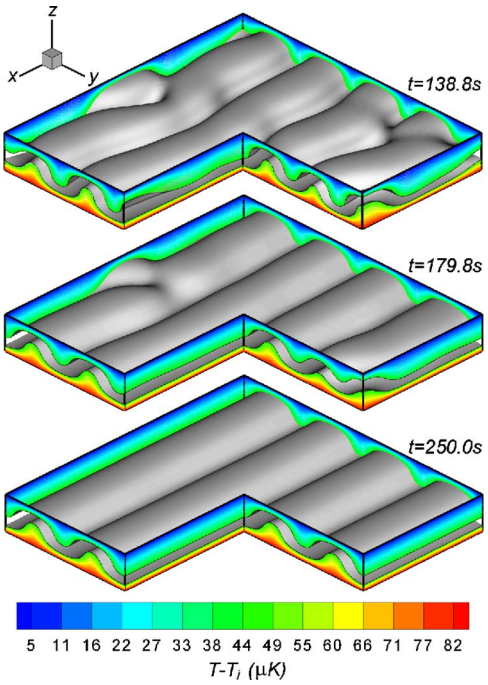

FIG. 4. (Color online) Cuts of the temperature fields for $\varepsilon=0.2$ and $q=0.216$ μW/cm^2 (unperturbed 3D solution). The lower and upper shaded isotherms correspond to T-$T_i=60$ and 30 μK, respectively. The temperature field at $t=250$ s corresponds to steady state (time-independent).

of the space-averaged enstrophy corresponding to the three simulations shown in Fig. 3. At the first instants of the simulation (not shown in Fig. 6), and before starting the heat, the enstrophy increases to reach a constant value. This value reflects the perturbation level of the dynamic field induced either by the numerical noise (for $B=0$) or by the inhomogeneous temperature field resulting from the diffusion of the additional perturbation applied on the top plate into the fluid layer (for $B\neq 0$).The flat signal of the enstrophy shown in Fig. 6 for $t<0$ indicates the saturation of the solution with perturbation. After the heating has started at $t=0$, ΔT increases, and when the instantaneous Rayleigh number, obtained from Eq. (1), exceeds the critical value $\mathrm{Ra}_c=1708$ (this occurs for $\Delta T=70.5$ μK at $t=6.7$ s), the intensity of

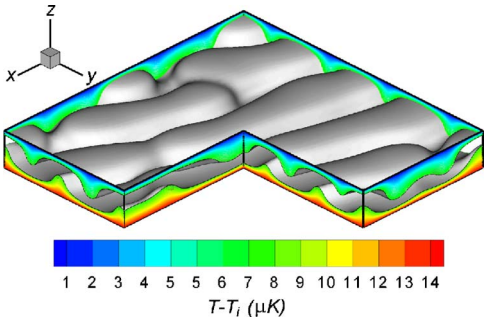

FIG. 5. (Color online) A cut of the steady-state (time-independent) temperature field for $\varepsilon=0.05$ and $q=45.8$ nW/cm^2 ($\mathrm{Ra}^{\mathrm{corr}}=4580$) (unperturbed 3D solution). The lower and upper shaded isotherms correspond to T-$T_i=10$ and 5 μK, respectively.

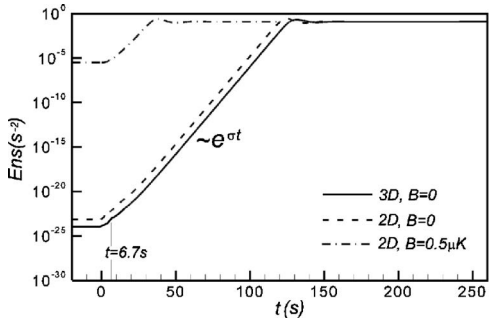

FIG. 6. Time evolutions of the space-averaged enstrophy [Eq. (2)] for $\varepsilon=0.2$ and $q=0.216$ μW/cm^2, with and without additional perturbation on the top plate. After the fluid layer has become unstable (at $t\sim 7$ s), the enstrophy increases exponentially with time.

convection increases exponentially with time until it produces enough convective transfer to noticeably deform the initially almost horizontal isotherms in the RB cell [13]. We note that the exponential growth rate of the convective activity (the slope σ of the curves before the convective regime) is the same in 2D and in 3D, with or without additional perturbation. Hence, for a given pair (ε,q), the value of t_p only depends on the perturbation level preceding the exponential growth phase of convection. This explains the slight difference of t_p between the 2D and the 3D solutions: for the same numerical parameters, the perturbation level in the 2D simulation is slightly higher than in its 3D counterpart. This also explains the large differences obtained with other 2D numerical studies and with the experiment: in the unperturbed 2D simulation, $t_p\sim 125$ s (see Fig. 3), compared with 90 s in [3] and 45 s in [2], while the experimental value is about 30 s. The development of the convective regime depends on the inherent noise of the simulation (truncations of large numbers in the code) or the experiment (nonideal RB cell). It appears hence that the earlier simulations [2,3] were inherently noisier than those in the present study. On the other hand, according to Fig. 6, for $B\neq 0$, the additional perturbation of the dynamic field, though small, is much larger than the noise level of numerical origin. Hence, with the additional perturbation, the value of t_p becomes independent of the numerical method used: for $B=0.5$ μK, $t_p=29.2$ s (Fig. 3) agrees closely with the value obtained numerically in [3] and it is also close to that from the experiment. Consequently, the perturbation level produced in the simulation with $B=0.5$ μK is comparable with that in the measurements due to the imperfections of the experimental conditions. Several 2D simulations were carried out for different amplitudes of the perturbation on the top plate. The value B_{best} of B for which $t_p=30$ s (its experimental value) is obtained by interpolation; $B_{\mathrm{best}}=0.39$ μK. This amplitude was then used to perturb the solutions for different combinations of ε and q.

IV. APPLICATION TO OTHER VALUES (ε,q)

As mentioned before, the exponential growth rate of convection σ is the same for both the 2D and the 3D simulations (see Fig. 6), as well as the value of ΔT_{ss} and consequently of

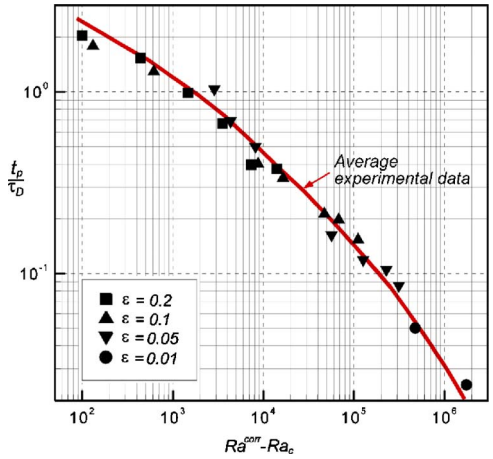

FIG. 7. (Color online) The time t_p (when the convective regime is developing), scaled by the thermal diffusion relaxation time τ_D, as a function of the steady-state Rayleigh number, for a temperature perturbation on the top plate with an amplitude $B=0.39$ μK.

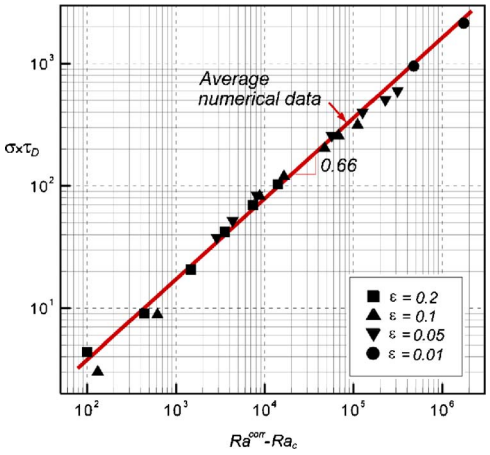

FIG. 9. (Color online) The exponential convection growth rate σ, scaled by the thermal diffusion relaxation rate τ_D^{-1} as a function of the steady-state Rayleigh number, with or without a temperature perturbation on the top plate.

the Rayleigh number [Eq. (1)]. This behavior was confirmed for other combinations of ε and q. Hence, the 2D approximation is adequate for providing the value of t_p, which will be nearly the same as in 3D. This is because the additional perturbation is much larger than the inherent noise of the unperturbed simulations, as shown in Fig. 6, and masks it. For each pair of parameters (ε,q), an unperturbed 2D simulation was carried out first in order to identify the natural convection wavelength of the solution. This specified the value of α in the expression of the additional temperature perturbation $T_{\text{top}}-T_i$ applied subsequently, with $B=B_{\text{best}}=0.39$ μK, on the top plate. Figure 7 shows the results of t_p/τ_D for many combinations of ε and q, as a function of the steady-state Rayleigh number. Here the simulation results are represented by symbols, while the solid line represents the average curve of the experimental data shown in Fig. 5(b) of Ref. [8]. The difference between the numerical and the experimental values of ΔT_{ss} never exceeded 6%, with a mean difference of 2.8%. We note first that for all values of ε, the values of t_p/τ_D collapse on a single curve. Such a scaling was justified by the simple model mentioned earlier [9].

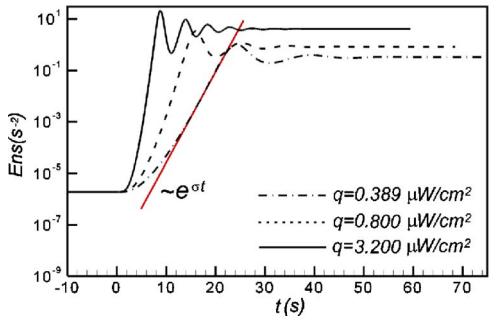

FIG. 8. (Color online) Time evolutions of the space-averaged enstrophy for $\varepsilon=0.2$ and for three values of the q (starting at $t=0$), with a temperature perturbation amplitude $B=0.39$ μK on the top plate. Here the red line indicates the limiting slope σ, observed beyond the curved portion that marks the instability beginning. Also σ increases with q.

Good agreement is now obtained between the experiments and the perturbed 2D simulations over more than four decades of the Rayleigh number. Thus, the additional perturbation removes the discrepancy for the value of t_p/τ_D between the experiments and earlier simulations shown in Fig. 5(b) of Ref. [8], which had been found to increase systematically with decreasing Ra^{corr}-Ra_c. Indeed, referring back to Fig. 4, we can show that $t_p^{B=0}$-$t_p^{B\neq 0}\approx\sigma^{-1}[\ln(\text{Ens}_0^{B=0})-\ln(\text{Ens}_0^{B\neq 0})]$, where Ens_0 is the mean enstrophy at the beginning of its exponential growth, which reflects the initial level of perturbation; hence for a given numerical method $(\text{Ens}_0^{B=0})$ and a given perturbation level $(\text{Ens}_0^{B\neq 0})$, $t_p^{B=0}$-$t_p^{B\neq 0}$ should increase with decreasing σ. On the other hand, Fig. 8 shows that, for a given ε, the time-growth rate of convection σ increases with q. Consequently, the time delay for the convective regime development, $t_p^{B=0}$-$t_p^{B\neq 0}$, increases with decreasing Ra^{corr}-Ra_c. In Fig. 9, a correlation is found empirically between the steady-state Rayleigh number and the scaled convection growth rate $\sigma\times\tau_D$. The limiting slope σ for each pair of values (ε,q) is defined in Fig. 8. Over approximately four decades in the Rayleigh number, $\sigma\times\tau_D$ is proportional to $(\text{Ra}^{\text{corr}}$-$\text{Ra}_c)^{2/3}$, a relation that needs to be explained.

V. CONCLUSIONS

3D and perturbation-controlled 2D numerical simulations of the convection onset in a Rayleigh-Bénard cell filled with ^{3}He have been reported. The satisfactory agreement obtained for the characteristic time t_p of the convective regime emergence indicates that an amplitude $B=0.39$ μK of the described perturbation is a good representation of the noise level in the experiment. The introduced artificial perturbation model must be interpreted as a measure of the effects of the cell's imperfections: the roughness and the alignment of the horizontal plates, the vertical walls effects, possible inhomogeneity of the heating, etc. The value of B_{best} is therefore representing the perturbations in the experimental Rayleigh-Bénard cell. Futhermore, the amplitude of the introduced

perturbation is consistent with the temperature fluctuations in the regulated top plate temperature in the experiment that are estimated to be of the order of $0.5\,\mu K$. The 3D simulations justify the relevance of the 2D approximation for finding the value of t_p, however the description of the flow structure and the temperature patterns requires 3D simulations.

Differences remain between the simulations and the experiments, for instance the amplitude and damping of the oscillations in $\Delta T(t)$. In particular, the truncated oscillations of the experimental $\Delta T(t)$ curve in Fig. 3 (which become damped oscillations at higher values of q) remain to be understood. In addition, the observed [8] slow relaxation time to steady state, τ_{tail}, is not detected in the simulations. Furthermore, the power-law representation of the scaled growth rate $\sigma \times \tau_D \sim (\text{Ra}^{\text{corr}}\text{-Ra}_c)^{2/3}$ needs to be understood.

ACKNOWLEDGMENTS

The authors acknowledge the financial support of the CNES and the computing resources of the IDRIS center.

[1] A. Furukawa and A. Onuki, Phys. Rev. E **66**, 016302 (2002).
[2] S. Amiroudine and B. Zappoli, Phys. Rev. Lett. **90**, 105303 (2003).
[3] A. Furukawa, H. Meyer, and A. Onuki, Phys. Rev. E **71**, 067301 (2005).
[4] A. B. Kogan and H. Meyer, Phys. Rev. E **63**, 056310 (2001).
[5] H. Meyer and A. B. Kogan, Phys. Rev. E **66**, 056310 (2002).
[6] B. Zappoli, D. Bailly, Y. Garrabos, B. Le Neindre, P. Guenoun, and D. Beysens, Phys. Rev. A **41**, 2264 (1990); B. Zappoli, Phys. Fluids A **4**, 1040 (1992); A. Onuki, *Phase Transition Dynamics* (Cambridge University Press, Cambridge, 2002), Sec. 6.3.
[7] M. Gitterman and V. Steinberg, High Temp. **8**, 754 (1970); P. Carlès and B. Ugurtas, Physica D **126**, 69 (1999).
[8] A. Furukawa, H. Meyer, A. Onuki, and A. B. Kogan, Phys. Rev. E **68**, 056309 (2003).
[9] H. Meyer, Phys. Rev. E **73**, 016311 (2006).
[10] S. Chandrasekar, *Hydrodynamic and Hydro-Magnetic Stability* (Dover Publications Inc., New York, 1981).
[11] G. Accary and I. Raspo, Comput. Fluids (to be published).
[12] Y. Dubief, F. Delcayre, J. Turbul. **1**, 011 (2000).
[13] For a first-principles calculation giving the shape of the growing perturbation in supercritical ^{3}He, see L. El Khouri and P. Carlès, Phys. Rev. E **66**, 066309 (2002).